

Critical phase boundaries of static and periodically kicked long-range Kitaev chain

Utso Bhattacharya¹, Somnath Maity¹, Amit Dutta¹ and Diptiman Sen²

¹*Department of Physics, Indian Institute of Technology, Kanpur 208016, India*

²*Centre for High Energy Physics, Indian Institute of Science, Bengaluru 560012, India*

We study the static and dynamical properties of a long-range Kitaev chain, i.e., a p -wave superconducting chain in which the superconducting pairing decays algebraically as $1/l^\alpha$, where l is the distance between the two sites and α is a positive constant. Considering very large system sizes, we show that when $\alpha > 1$, the system is topologically equivalent to the short-range Kitaev chain with massless Majorana modes at the ends of the system; on the contrary, for $\alpha < 1$, there exist symmetry protected massive Dirac end modes. We further study the dynamical phase boundary of the model when periodic δ -function kicks are applied to the chemical potential; we specially focus on the case $\alpha > 1$ and analyze the corresponding Floquet quasienergies. Interestingly, we find that new topologically protected massless end modes are generated at the quasienergy π/T (where T is the time period of driving) in addition to the end modes at zero energies which exist in the static case. By varying the frequency of kicking, we can produce topological phase transitions between different dynamical phases. Finally, we propose some bulk topological invariants which correctly predict the number of massless end modes at quasienergies equal to 0 and π/T for a periodically kicked system with $\alpha > 1$.

I. INTRODUCTION

Topological phases of quantum condensed matter systems have been extensively studied for the past several years¹⁻³. Typically, these are phases in which the system is gapped and insulating in the bulk but has gapless modes at the boundaries which can contribute to transport at low temperatures. Further, the number of species of gapless boundary modes is given by a topological invariant whose nature depends on the spatial dimensionality of the system and the symmetries that it possesses, such as chiral symmetry, particle-hole symmetry and time-reversal symmetry. The significance of a topological invariant is that it does not change if the system is perturbed as long as the bulk modes remain gapped and the symmetry of the system remain unaffected by the perturbation. Two- and three-dimensional topological insulators, quantum Hall systems, and one-dimensional wires with p -wave superconductivity provide some examples of topological phases.

More recently, there has been considerable interest in exploring topological features associated with periodically driven closed quantum systems⁴⁻²⁷. Boundary modes and topological invariants have been studied in this context^{4-6,10,17-20,22}. A photonic topological insulator has been demonstrated experimentally where a two-dimensional lattice of helical waveguides has been shown to exhibit topologically protected end modes²⁸. However, the existence of topological invariants and the relation between them and the number of Majorana modes at the boundary seems to be unclear, particularly if the driving frequency is small¹⁸. Further, the Majorana boundary modes are of two types (corresponding to eigenvalues of the Floquet operator being equal to $+1$ or -1). In a recent study of a periodically driven one-dimensional short-range Kitaev (SRK) chain²⁹, it has been shown that the numbers of these two types of modes can be obtained from a topological invariant²⁷. In some variations of the

Kitaev chain, end modes corresponding to Floquet eigenvalues *not* equal to ± 1 are found³⁰; it is not known if there are topological invariants which can describe such modes.

In this paper, we will study in detail one-dimensional p -wave superconductors with long-range pairings. We will first revisit its static phase diagram and then investigate the dynamical generation of end modes under periodic kicking of the chemical potential. We will elaborate on how the presence of long-range pairings modify the properties of both the static and the dynamical systems, especially in comparison with the corresponding short-range systems²⁷.

Let us recall that topological superconductors are expected to host massless Majorana modes which obey non-Abelian statistics and can therefore serve as essential components of a topological quantum computer. The most important feature of such topological systems is the existence of robust gapless boundary modes which are immune to disorder. There have been a number of experiments recently which have found signatures of Majorana modes in one-dimensional or quasi-one-dimensional systems³¹.

Considering the relevance and immense interest in realizing topological superconductors, the Kitaev chain which is a paradigmatic model exhibiting topological superconducting phases has been studied in the presence of long-range superconducting pairings³²⁻³⁶ to determine which specific properties of a model are necessary for such phases to occur. In this model, the superconducting pairing is taken to decay as $1/l^\alpha$, where l is the distance between the two sites. It has been reported that there are three different topological phases depending upon the power-law exponent α which characterizes the pairing. For $\alpha > 3/2$, it has been established that the model is topologically equivalent to the SRK chain with nearest-neighbor pairing terms. However, for $\alpha < 1$, the emergence of a new topological phase has been noted which

hosts massive Dirac fermionic end modes that lie within the bulk energy gap and are topologically robust³⁵. Most intriguing is the presence of a crossover region that interpolates smoothly between the $\alpha < 1$ and the $\alpha > 3/2$ regions. To better understand the behavior of the crossover region, we have performed exact diagonalization for large system sizes in this paper to establish that the crossover region $1 < \alpha < 3/2$ only exists as a consequence of the system size being taken to be finite in earlier papers. We exhibit that in the thermodynamic limit of the system size $L \rightarrow \infty$, this intermediate region is also topologically equivalent to the SRK chain characterized by a well-defined topological invariant which is a winding number and is always an integer. Therefore there are only two different regions: a short-range model for $\alpha > 1$ and a long-range model for $\alpha < 1$.

To attain further control over topological phases of matter, one sometimes considers periodically driven systems governed by the Floquet theorem. The periodic driving offers such an immense control over topological phases that it shows considerable promise as a viable approach towards creating topological materials with high tunability and engineering new non-equilibrium topological phases which are absent in their static counterparts. For instance, Majorana end modes can be generated in a one-dimensional p -wave superconducting system, by varying the chemical potential through some periodic δ -function kicks with time²⁷. Motivated by these considerations, we investigate in this paper how the topological properties of the Kitaev chain get modified in the presence of both periodic kicking and long-range superconducting pairing with a power-law decay and whether some exotic topological phases emerge in this driven system.

The outline of this paper is as follows. In Sec. II we introduce the system of interest and review some of its properties. The system we consider is a tight-binding model of spinless electrons with a long-range p -wave superconducting pairing and a chemical potential μ ; this is called the long-range Kitaev (LRK) chain. In Sec. III, we discuss the energy spectrum, the phase boundaries and the topological and non-topological phases that this model possesses. In this process we establish the phase diagram of the LRK chain and we illustrate that it consists of two regions based on the value of α : (i) for $\alpha > 1$, the LRK chain is effectively short-ranged and has topological phases which are characterized by a topological invariant (winding number) given by $\nu = 1$ and host massless (zero energy) Majorana modes at the ends of a long system for $-1 < \mu < 1$, while (ii) for $\alpha < 1$, the long-range pairing gives rise to topological phases which have winding number given by $\nu = 1/2$ and host massive Dirac modes at the ends for $\mu > -1$ ³⁵. On the other hand, the system has topologically trivial phases which have no end modes for $|\mu| > 1$ if $\alpha > 1$ and $\mu < -1$ if $\alpha < 1$; these phases are characterized by a winding number equal to 0 and $-1/2$ respectively. In Sec. IV, we discuss our analytical method of studying the Floquet evolution and derive

the Floquet Hamiltonian when the the chemical potential is driven by periodic δ -function kicks which obey all the symmetries of the static Hamiltonian³⁷. In Sec. V, we study the quasienergy spectrum versus the chemical potential for various values of the system parameters and show that new topological phases emerge. We also establish the critical gap closing points for certain ranges of α before discussing the ubiquitous features generated by the periodic kicking. In Sec. VI, we study the ranges of parameters in which massless Majorana and massive end modes appear at the ends of an open system. We then use the Floquet operator for a system with periodic boundary conditions to define some topological invariants and show that they correctly predict the numbers of end modes with Floquet eigenvalues equal to $+1$ and -1 for the $\alpha > 1$ region. We find that end modes can either appear or disappear as the driving frequency is varied. Finally we summarize our main results and point out some directions for future work in Sec. VII.

II. KITAEV CHAIN WITH LONG-RANGE SUPERCONDUCTING PAIRING

We consider a model of spinless fermions on a one-dimensional chain with long-range p -wave superconducting pairings; this is known as the LRK chain. For a system with L sites and periodic boundary conditions, the Hamiltonian has the form³²

$$H = \sum_{n=1}^L \left\{ \gamma \left(c_{n+1}^\dagger c_n + c_n^\dagger c_{n+1} \right) - \mu \left(2c_n^\dagger c_n - 1 \right) + \sum_{l=1}^{L-1} \frac{\Delta}{d_l^\alpha} \left(c_{n+l}^\dagger c_n^\dagger + c_n c_{n+l} \right) \right\}, \quad (1)$$

where $\gamma > 0$ is the hopping amplitude, μ is the chemical potential, Δ is the superconducting pairing amplitude, and c_n (c_n^\dagger) are fermionic annihilation (creation) operators defined at site n of the chain. (We will assume that both γ and Δ are real and positive; μ can be positive or negative). The superconducting pairing is a function of the distance $d_l = \text{Min}[l, L-l]$ between the two sites n and $n+l$; it is long-range since it decays as a power-law with an exponent $\alpha > 0$. Although the Hamiltonian does not conserve the total fermionic number, the parity operator (total fermionic number modulo two) commutes with the Hamiltonian and is conserved.

For both periodic and open boundary conditions, the Hamiltonian in Eq. (1) can be written in terms of Majorana operators. The Majorana operators are defined as follows,

$$\begin{aligned} a_{2n-1} &= c_n + c_n^\dagger, \\ a_{2n} &= i(c_n - c_n^\dagger). \end{aligned} \quad (2)$$

It is easy to verify that these are Hermitian operators satisfying $\{a_m, a_n\} = 2\delta_{mn}$. Using these operators, we can

rewrite the Hamiltonian (Eq. (1)) with open boundary conditions as

$$H = \sum_{n=1}^{L-1} \left[\frac{i\gamma}{2} (a_{2n}a_{2n+1} - a_{2n-1}a_{2n+2}) - \frac{i\Delta}{2} \sum_{l=1}^{L-n} \frac{1}{l^\alpha} (a_{2n}a_{2n+2l-1} + a_{2n-1}a_{2n+2l}) \right] + i\mu \sum_{n=1}^L a_{2n-1}a_{2n}. \quad (3)$$

We first discuss the well established extreme short-range limit ($\alpha \rightarrow \infty$)²⁹ of Eq. (3). There are two phases present in this limit: a trivial phase for $|\mu| > 1$, and a topological phase for $-1 < \mu < 1$. In the topological phase, there is one Majorana zero mode (MZM) at each end of an infinitely long open chain. (If the chain is not infinitely long, the modes at the two ends hybridize and their energies shifts from away zero; then the modes do not have a Majorana character). The two MZMs can together be written in terms of an ordinary fermion operator (for which $c \neq c^\dagger$); the corresponding zero energy state may be occupied or unoccupied ($c^\dagger c = 1$ or 0). This gives rise to two possible ground states which are degenerate for an infinitely long chain. Hence the ground state of the SRK chain is two-fold degenerate, but the two states have different parities depending on whether the zero energy state is occupied or not. For instance, if the bulk has an even number of occupied states, the two possible parity sectors are given by (i) states where the MZM is unoccupied resulting in even fermion parity, and (ii) states where the MZM is occupied giving rise to odd fermion parity. We will show below that the LRK chain remains effectively short-ranged as long as the decay exponent $\alpha > 1$; this is in contrast to the results obtained in Ref. 35.

Without loss of generality, we will set $\gamma = -\Delta = 1$ in the rest of this paper. If we assume periodic boundary conditions, the translational symmetry of the system enables us to implement a Fourier transformation and rewrite the Hamiltonian in the Nambu spinor basis given by $\psi_k = (c_k, c_{-k}^\dagger)^T$. In the thermodynamic limit $L \rightarrow \infty$, the momentum k becomes a continuous variable lying in the interval $[-\pi, \pi]$, and we get^{32,33,35},

$$H = \int_{-\pi}^{\pi} \frac{dk}{2\pi} \Psi_k^\dagger H_k \Psi_k, \quad (4)$$

where

$$H_k = -f_\alpha(k) \sigma^y + (\cos k - \mu) \sigma^z, \quad (5)$$

and

$$f_\alpha(k) = \sum_{l=1}^{\infty} \frac{\sin(kl)}{l^\alpha}. \quad (6)$$

This is related to the polylogarithm function $Li_\alpha(z) \equiv$

$\sum_{l=1}^{\infty} z^l/l^\alpha$ as

$$f_\alpha(k) = -\frac{i}{2} (Li_\alpha(e^{ik}) - Li_\alpha(e^{-ik})). \quad (7)$$

The eigenvalues of the Hamiltonian in Eq. (5) are

$$E_k^\pm = \pm \sqrt{(\cos k - \mu)^2 + (f_\alpha(k))^2}. \quad (8)$$

To simplify the notation, we now rewrite the Hamiltonian in terms of a unit vector \hat{n}_k so that H_k takes the form

$$H_k = \Delta_k \hat{n}_k \cdot \vec{\sigma}, \quad (9)$$

where $\vec{\sigma} = (\sigma^x, \sigma^y, \sigma^z)$ are the Pauli matrices, and

$$\begin{aligned} \Delta_k &= |E_k^\pm|, \\ \hat{n}_k &= \frac{1}{\Delta_k} (0, -f_\alpha(k), \cos k - \mu). \end{aligned} \quad (10)$$

It is worth noting that the LRK chain lies in the BDI symmetry class of topological insulators and superconductors^{38,39}, and is particle-hole, time-reversal, and chiral symmetric. These symmetries restrict the movement of the vector \hat{n}_k from a sphere S_2 in three dimensions to a circle S_1 in the $y-z$ plane; this leads to a mapping from the Hamiltonians H_k in the Brillouin zone $k \in S_1$ to the winding vector $\hat{n}_k \in S_1$. This mapping, for a short-ranged interacting system, yields a Z -valued topological invariant called the winding number ν which is the angle subtended by \hat{n}_k when the momentum k goes from $-\pi$ to π . We find that

$$\nu = \frac{1}{2\pi} \oint dk \frac{\partial_k n_k^y}{n_k^z}. \quad (11)$$

Alternatively, the same winding number can be obtained by considering an adiabatic transport of the system from a certain crystal momentum through a reciprocal lattice vector. After making the Hamiltonian in Eq. (9) off-diagonal by a unitary rotation, the eigenstate in the lower band, $|g_k\rangle = (u_k, v_k)^T$, then picks up a Berry/Zak phase⁴⁰⁻⁴² defined as

$$\phi_Z = i \oint dk \langle g_k | \partial_k | g_k \rangle. \quad (12)$$

This is generally quantized in integer multiples of π and has a one-to-one correspondence with the winding number defined in Eq. (11).

III. PHASE DIAGRAM

In order to determine the topological phase diagram of this system, we find the critical lines of the Hamiltonian by considering the thermodynamic limit $L \rightarrow \infty$. The critical lines are obtained by studying the zeros and divergences of the function $f_\alpha(k)$ in Eq. (6) which encodes all the information about the long-range pairing. It is evident that when $\alpha > 1$, $f_\alpha(k_c) = 0$ for the critical momenta $k_c = 0$ and π , but when $\alpha \leq 1$, $f_\alpha(k_c) = 0$ only for $k_c = \pi$. For $\alpha < 1$, $f_\alpha(k)$ diverges at zero momentum i.e., $f_\alpha(k) \rightarrow \infty$ as $k \rightarrow 0$. This leads to a divergence of the energy in Eq. (8) which scales with momentum as $E_k^\pm \sim k^{-(1-\alpha)}$. We thus see that for $\alpha > 1$, the energy goes to zero for both $k_c = 0, \pi$; hence both the lines $\mu = \pm 1$ are critical. On the contrary, due to the divergence of the energy at $k = 0$ for $\alpha \leq 1$, only the line $\mu = -1$ is critical. Therefore, according to the behavior of $f_\alpha(k)$ at $k = 0$, the existence of two different topological phases depending on the exponent α are obtained as follows.

(a) The $\alpha > 1$ region is equivalent to the topological phase of the SRK chain²⁹ as we will show below. The $|\mu| > 1$ phase is topologically trivial and is marked by the absence of MZMs. On the other hand, MZMs are present for $-1 < \mu < 1$. The presence of a phase discontinuity at $k = 0$ in the ground state eigenvector $|g_k\rangle$ and the function $f_\alpha(k)$ being non-divergent yields the invariant $\nu = \phi_Z/\pi = 1^{35}$. More generally, the winding number $\nu = 1$ for $-1 < \mu < 1$ and is zero otherwise, in the entire region $\alpha > 1$.

To probe the behavior of the topological end modes in the $\alpha > 1$ region, we will consider the two sub-regions $\alpha > 3/2$ and $1 < \alpha < 3/2$. We first look at the region $\alpha > 3/2$. It is straightforward to numerically ascertain through the plots of the energy spectrum versus μ with open boundary conditions, that the region $\alpha > 3/2$ is effectively short-ranged. In the plot of the energy spectrum E against μ in Fig. 1(a), we notice that there is a slight gap in the energy spectrum around $\mu = 1$; however this is an artefact of the relative smallness of the system size $L = 60$ chosen. Upon increasing the system size to $L = 1000$ in (Fig. 1(b)), we see that the slight energy gap at $\mu = 1$ disappears up to numerical precision. This establishes that the energy spectrum for $\alpha > 3/2$ is topologically equivalent to the SRK chain as it hosts MZMs for $-1 < \mu < 1$ and is non-topological otherwise.

Next, we will look at the region $1 < \alpha < 3/2$. We will show that this also hosts MZMs for $-1 < \mu < 1$. However this range of α deserves special attention. This is because the group velocity $v_g = \partial_k E_k^\pm$ scales as $v_g \sim k^{-(3-2\alpha)}$ as $k \rightarrow 0$ and diverges for all μ , whereas such a divergence of v_g is absent when $\alpha > 3/2$.

In Fig. 2(a), we have plotted the energy spectrum E of the LRK chain with open boundary conditions versus the chemical potential μ for $\alpha = 1.4$ for a small system size $L = 60$. This figure seems to imply that there are three

topologically distinct phases depending on the value of μ : trivial with no end modes for $\mu < -1$ and $\mu > 1$, and massless Majorana end modes and massive Dirac end modes (MDMs) which lie within the bulk gap for $-1 < \mu < 1$. The Dirac-like end modes with energy slightly away from zero are visible near $\mu = 1$. Thus the energy spectrum found observed for a small system size like $L = 60$ appears to exhibit a crossover-like behavior around $\mu = 1$ where the energies of some end modes move away from zero and merge with the bulk bands. However this view of the spectrum is misleading. Since the group velocity v_g diverges at $k = 0$ as $k^{-(3-2\alpha)}$, the energy spectrum becomes highly dispersive; for a finite size system in which k is quantized in units of $2\pi/L$, the difference between the energies for two neighboring values of k diverges near $k = 0$. Therefore, it takes an ever increasing system size L to realize that a crossover region does not really exist in the thermodynamic limit $L \rightarrow \infty$. In Fig. 2(b), we show the energy spectrum E of the LRK chain with open boundary conditions for $\alpha = 1.4$ and a much larger system size with $L = 1000$. It is now clear that the apparent crossover behavior observed for $L = 60$ near $\mu = 1$ has vanished; there are no MDMs at any value of μ . However, MZMs are present for $-1 < \mu < 1$ establishing that for $1 < \alpha < 3/2$, the energy spectrum topologically resembles that of a SRK chain.

To establish more conclusively the effectively short-ranged behavior of the model with $1 < \alpha < 3/2$ in the thermodynamic limit, we show in Fig. 2(c) that for $-1 < \mu < 1$, the end modes become MZMs. The masslessness of the end modes in the region $-1 < \mu < 1$ is verified by observing the variation of the mass gap (lowest positive eigenvalue E_1 minus zero) with the inverse of system size, $1/L$, for two values of μ lying in this region. Although for a small system size $L = 10$, there is a finite mass gap, the mass gap decreases with increasing system size and approaches zero for $L \rightarrow 5000$. The energy spectrum for $|\mu| < 1$ would therefore host MZMs in the $L \rightarrow \infty$ limit. For $\mu > 1$, the difference between the lowest positive eigenvalue E_1 from the second lowest positive eigenvalue E_2 has been plotted versus $1/L$ in Fig. 2(d). Although $E_2 - E_1$ is finite for $L = 10$, the gap decreases with increasing system size as L approaches the thermodynamic limit, showing that the MDMs merge with the bulk spectrum in the thermodynamic limit. Hence MDMs which would live near the ends of the system and would be separated from the bulk modes do not survive in the limit $L \rightarrow \infty$. Thus there are no end modes for $\mu > 1$. This makes the short-ranged nature evident for the entire range of values of $\alpha > 1$.

(b) We now focus our attention on the region $\alpha < 1$ which is truly an emergent feature of the long-range nature of the superconducting pairing; here the phase diagram is expected to be drastically different from the conventional SRK model. In this region, for all $\mu < -1$ the system with open boundary conditions

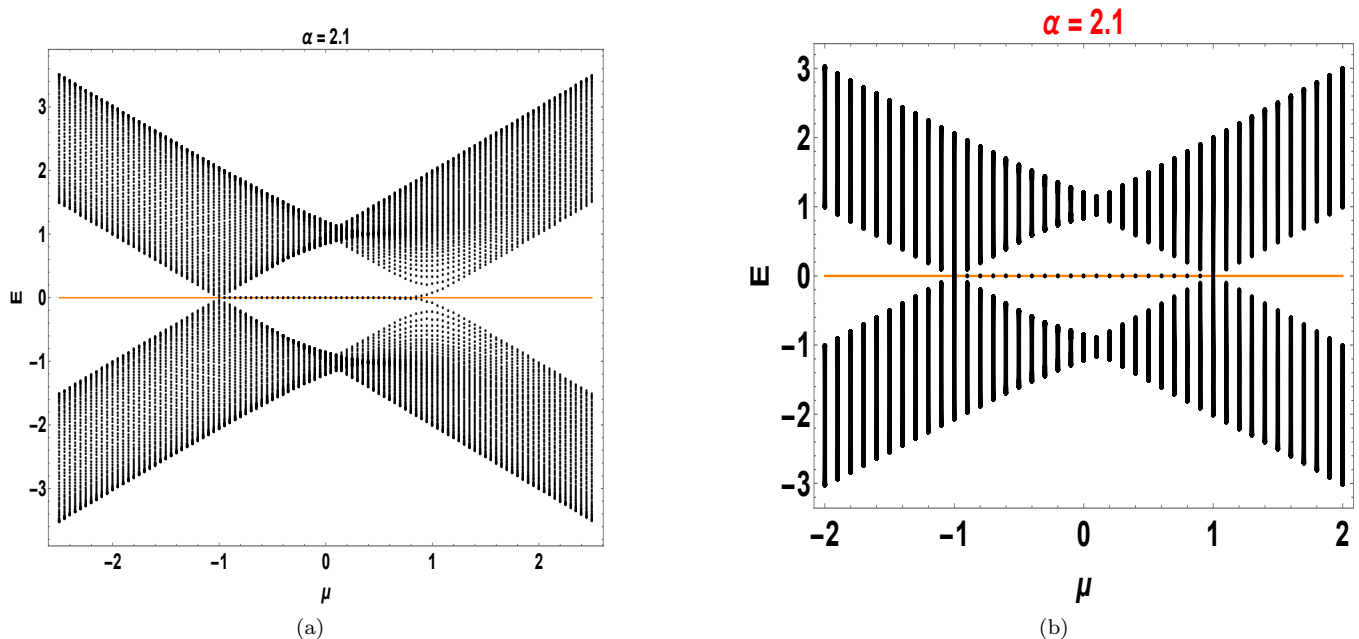


FIG. 1: (a) Energy spectrum E of the LRK chain with open boundary conditions plotted versus the chemical potential μ for $\alpha = 2.1$ and system size $L = 60$. We see that there is a slight energy gap at $\mu = 1$. (b) Energy spectrum E for the same value of $\alpha = 2.1$ but with a much larger system size $L = 1000$. On increasing the system size we see that the slight energy gap at $\mu = 1$ has disappeared, up to numerical precision. The energy spectrum for this value of α is topologically equivalent to the SRK chain as it hosts zero energy Majorana modes for $-1 < \mu < 1$ and is non-topological otherwise.

is in a trivial phase with no end modes, while for all $\mu > -1$, this system hosts topological MDMs at the ends (see Fig. 3(a)). These MDMs appear due to the coupling induced between the two MZMs at the two distant ends due to the presence of long-range pairing; hence the MDM formed is a highly non-local object. Moreover, although the Dirac mode is massive, it is still topological and is protected by the bulk gap. This non-local topological quasiparticle is also protected by the fermionic parity because the ground state of the system in this phase still retains its even parity; populating the MDM which is the first excited state of the system would then require a change in the fermionic parity from even to odd. Since no discrete symmetry has been broken by the inclusion of the long-range pairing, the system still belongs to the BDI symmetry class. However, the winding number ν is modified by the topological singularity at $k = 0$ generated by the long-range pairing. This happens because at $k = 0$ both the energy dispersion E_k^\pm in Eq. (8) and the group velocity $\partial_k E_k^\pm$ diverge as the integrand in the definition of the Berry/Zak phase in Eq. (12) is considered in the limit $k \rightarrow 0$. For the trivial phase with $\mu < -1$, the winding number is $\nu = -1/2$, whereas in the topological phase hosting MDMs which occurs for $\mu > -1$, it turns out that $\nu = +1/2$. Although the topological invariant is a half-integer in both cases, the difference between the invariants in the two topologically different phases is unity, indicating that a topological phase transition

separates the two half-integer quantized topological phases. The parameter range $\alpha < 1$ is thus in perfect agreement with the results of Ref. 35.

We will now ascertain whether the energy eigenvectors whose energies lie in the gap of the bulk bands are localized or not. A convenient numerical method for checking this is to look at the inverse participation ratio (IPR) for different values of α and μ . We assume that the eigenvectors of the open chain Hamiltonian in Eq. (3), denoted as $|e_j\rangle$, are normalized so that $\sum_{m=1}^{2L} |e_j(m)|^2 = 1$ for each value of j ; here $m = 1, 2, \dots, 2L$ labels the Majorana components a_m of the eigenvector $|e_j\rangle$. The IPR of an eigenvector is then defined as, $I_j = \sum_{m=1}^{2L} |e_j(m)|^4$. If $|e_j\rangle$ is extended equally over all sites so that $|e_j(m)|^2 = 1/(2L)$ for each m , then $I_j = 1/(2L)$ will approach zero in the thermodynamic limit. But if $|e_j\rangle$ is localized over a decay length ξ and remains constant as $L \rightarrow \infty$, then $|e_j(m)|^2 \sim 1/\xi$ in a region of length ξ and ~ 0 elsewhere. This yields $I_j \sim 1/\xi$ which will remain finite as $L \rightarrow \infty$. If L is sufficiently large, a plot of I_j versus j will be able to distinguish between states which are localized (over a length scale $\ll L$) and states which are extended. Therefore, to identify whether localized states exist in the various topological phases of the LRK chain, we plot the maximum value of the IPR, $\text{Max}[I_j]$, amongst all the states j versus the inverse of the system size ($1/L$); this is shown in Fig. 4. In the same figure, we

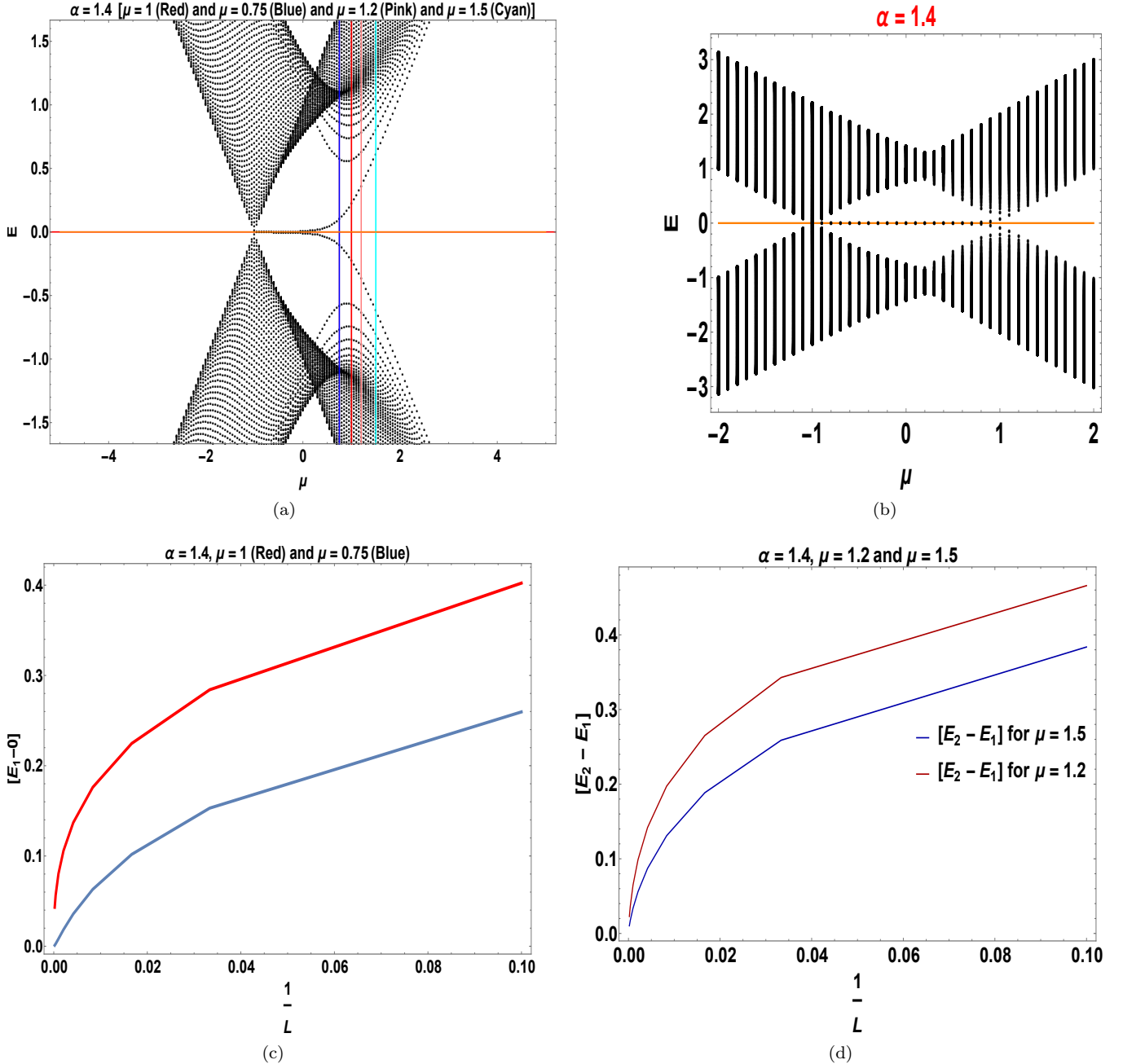


FIG. 2: (a) Energy spectrum E of the LRK chain with open boundary conditions plotted versus the chemical potential μ for $\alpha = 1.4$ and for a small system size $L = 60$. Three topological phases seem to exist depending on the value of μ : trivial with no end modes for $\mu < -1$, MZMs for $-1 < \mu \lesssim 0.5$, and MDMs for $\mu \gtrsim 0.5$. The blue, red, pink, cyan vertical lines lie at $\mu = 0.75, 1, 1.2, 1.5$ respectively. The spectrum apparently exhibits a crossover-like behavior for $\mu \gtrsim 0.5$. (b) Energy spectrum E of the LRK chain for the same value of $\alpha = 1.4$ but with a much larger system size $L = 1000$. The apparent crossover region observed for $L = 60$ (Fig. (a)) has almost completely vanished for $\mu > -1$, and there are almost no MDMs for any μ . MZMs are however present for $-1 < \mu < 1$ establishing that for $\alpha = 1.4$, the energy spectrum topologically resembles that of a SRK chain. (c) Deviation of mass gap (lowest positive eigenvalue E_1) from zero plotted versus the inverse of system size $1/L$ for two values of μ within the range $-1 < \mu < 1$. Although for a small system size $L = 10$, there is a finite mass gap, the gap reduces with increasing system size and approaches zero for $L \rightarrow 5000$. The energy spectrum for $\mu = 0.75$ (blue) and $\mu = 1$ (red) would thereby host MZMs in the $L \rightarrow \infty$ limit. (d) The difference between the lowest two positive eigenvalues, E_2 and E_1 , plotted versus $1/L$ to show how the MDMs merge with the bulk spectrum in the thermodynamic limit for two values of $\mu > 1$, $\mu = 1.2$ (red) and $\mu = 1.5$ (blue). Although $E_2 - E_1$ is finite for a small system size $L = 10$, the difference decreases with increasing system size as L approaches 5000. We therefore conclude that there would be no MDMs for $L \rightarrow \infty$.

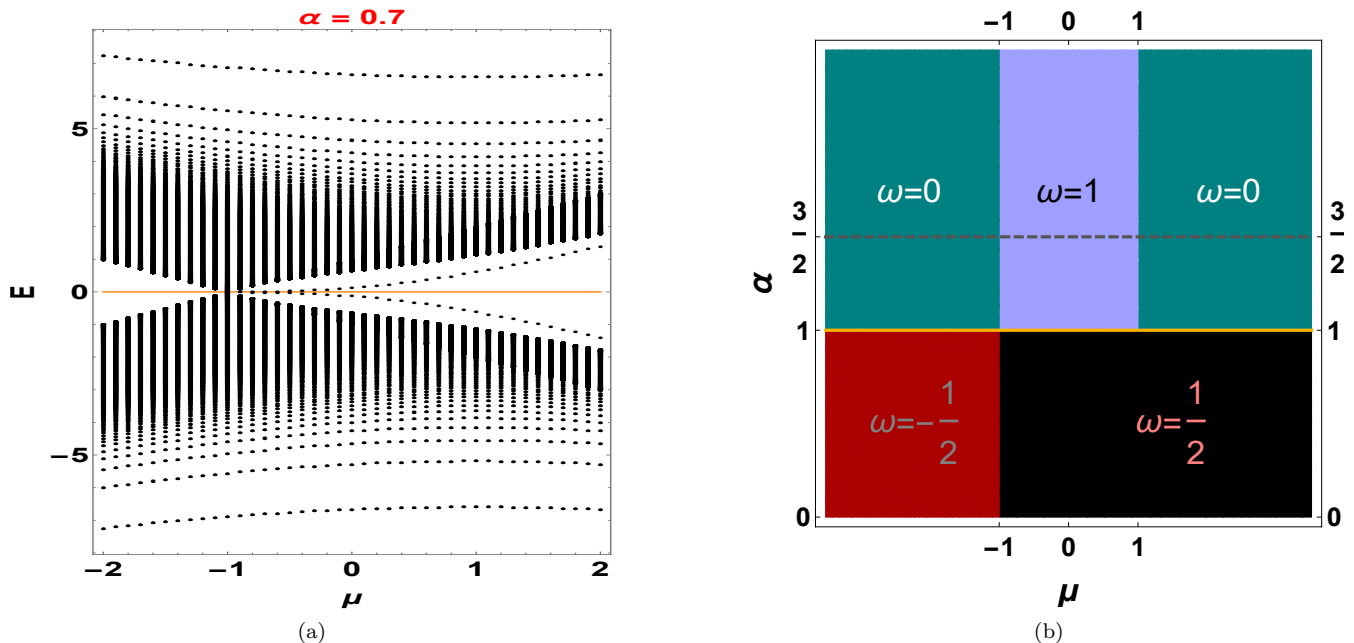


FIG. 3: (a) Energy spectrum E of the LRK chain with open boundary conditions plotted versus the chemical potential μ for $\alpha = 0.7$ and system size $L = 1000$. We see that there are no end modes lying in the bulk energy gap at $\mu \leq -1$. (b) Phase diagram of the LRK chain in the $\mu - \alpha$ plane. For $\alpha > 1$, the phase diagram is topologically equivalent to the SRK chain with three phases: two non-topological phases with $\nu = 0$ and a topological phase for $-1 < \mu < 1$ which has $\nu = 1$ and hosts MZMs at the ends of the system. For $\alpha < 1$, the model has a non-topological phase for $\mu < -1$ with $\nu = -1/2$ and a topological phase for $\mu > -1$ which has $\nu = 1/2$ and hosts MDMs at the ends.

also show how the difference between the maximum and the mean of the IPR, $\text{Max}[I_j] - \text{Mean}[I_j]$, scales with $1/L$. If both $\text{Max}[I_j]$ and $\text{Max}[I_j] - \text{Mean}[I_j]$ converge to finite non-zero values which are close to each other with increasing system size L , it confirms the presence of a localized mode. In all such cases, we have verified numerically that the maximum value of the IPR coincides with the IPR of an eigenstate whose energy eigenvalue lies within the bulk gap of the system. On the other hand, if both $\text{Max}[I_j]$ and $\text{Max}[I_j] - \text{Mean}[I_j]$ approach zero as $1/L \rightarrow 0$, it confirms the absence of any localized modes in the system.

To summarize, the phase diagram (see Fig. 3(b)) of the LRK chain consists of two regions depending on the value of α : (i) the region $\alpha > 1$ is effectively short-ranged and hosts massless MZMs for $-1 < \mu < 1$ where the winding number is $\nu = 1$, and (ii) the region $\alpha < 1$ where the effects of long-range pairings couple the two end modes together for all $\mu > -1$, thereby generating topologically robust MDMs. Interestingly, this phase is characterized by a winding number $\nu = 1/2$. The system lies in a topologically trivial phase with no end modes for $\alpha > 1$ and $|\mu| > 1$ where the winding number is zero, and also for $\alpha < 1$ and $\mu < -1$ where the winding number is $-1/2$.

IV. FLOQUET EVOLUTION: PERIODIC δ -FUNCTION KICKS IN CHEMICAL POTENTIAL

In this section, we consider what happens when the chemical potential μ is given δ -function kicks periodically in time. One reason for choosing to consider periodic kicks is that this is known to produce interesting effects in quantum systems such as dynamical localization³⁷. We will also see that the effects of periodic kicks are considerably easier to study both numerically and analytically compared to the case where μ varies harmonically with time. We will take the chemical potential in Eq. (1) to be of the form

$$\mu(t) = \mu + V \sum_{n=-\infty}^{\infty} \delta(t - nT), \quad (13)$$

where V is the kicking strength, $T = 2\pi/\omega$ is the time period and ω is the frequency of kicking. Eqs. (1) and (13) imply that the system has time-reversal symmetry: $H^*(-t) = H(t)$ for all values of t . (In general, we note that a system is said to have time-reversal symmetry if we can find a time t_0 such that $H^*(t_0 - t) = H(t)$ for all t , and does not have time-reversal symmetry if no such t_0 exists). As discussed below, we numerically compute the time evolution operator $U(T, 0)$ for periodic kicking for various values of the parameters γ , Δ , α , μ , V , ω and

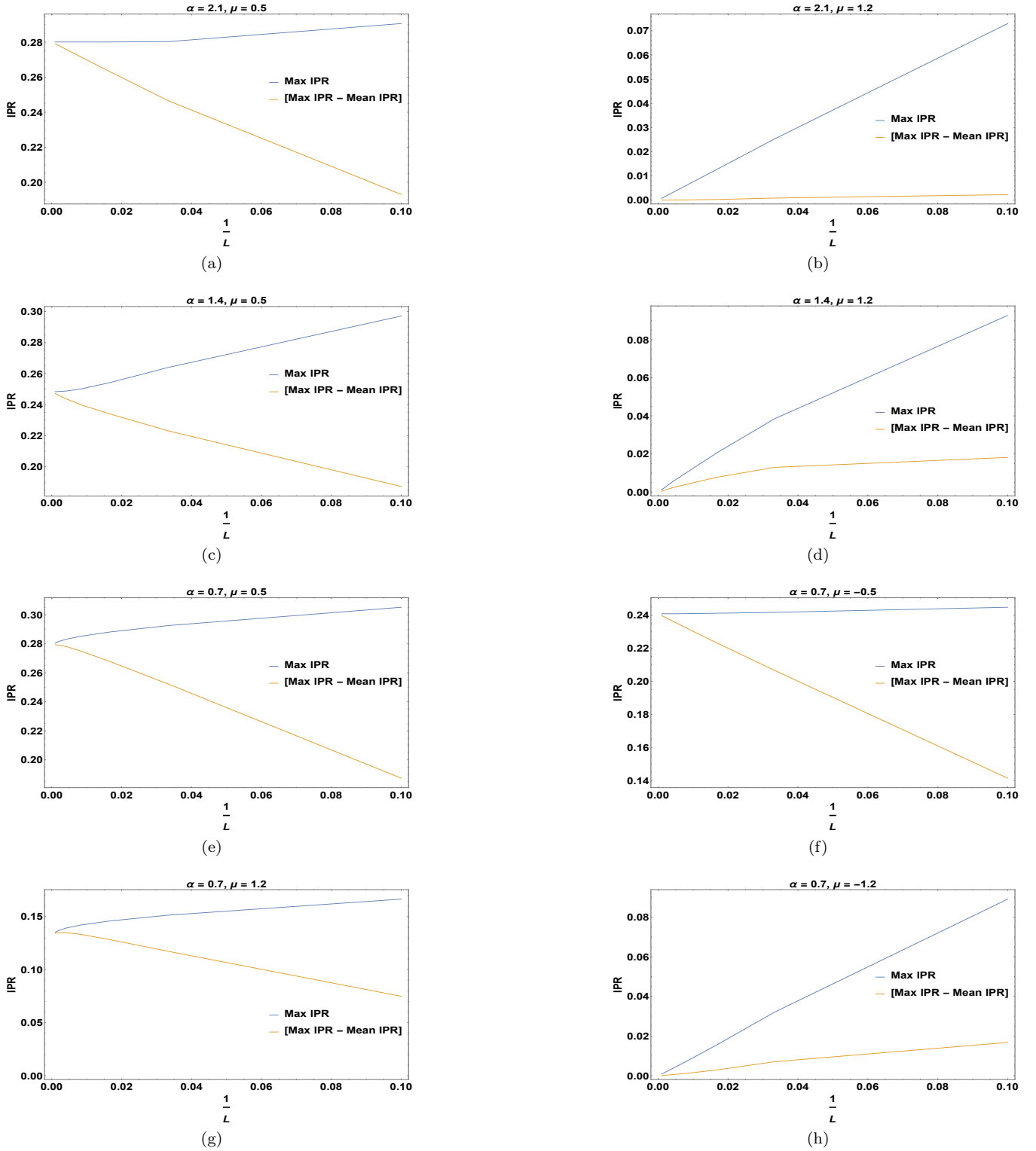


FIG. 4: Maximum value of the IPR ($\text{Max}[I_j]$ in blue) and the difference between the maximum and mean values of the IPR ($\Delta I_j = \text{Max}[I_j] - \text{Mean}[I_j]$ in yellow) plotted versus the inverse system size $1/L$. (a) For $\alpha = 2.1$ and $\mu = 0.5$, both $\text{Max}[I_j]$ and ΔI_j converge to a finite non-zero value with decreasing $1/L$ indicating that localized end modes are present. (b) For $\alpha = 2.1$ and $\mu = 1.2$, both $\text{Max}[I_j]$ and ΔI_j approach zero with decreasing $1/L$ indicating the absence of localized end modes. (c) For $\alpha = 1.4$ and $\mu = 0.5$ (these values are selected from the apparent crossover region), both $\text{Max}[I_j]$ and ΔI_j converge to a finite non-zero value with decreasing $1/L$ indicating that localized end modes are present. (d) For $\alpha = 1.4$ and $\mu = 1.2$, both $\text{Max}[I_j]$ and ΔI_j approach zero with decreasing $1/L$ indicating the absence of localized end modes once again. For $\alpha = 0.7$, the presence of (massive) localized end modes have been confirmed for (e) $\mu = 0.5$, (f) $\mu = -0.5$ and (g) $\mu = 1.2$, by observing a finite non-zero value of $\text{Max}[I_j]$ and ΔI_j as $1/L \rightarrow 0$, whereas localized end modes of any kind are absent for (h) $\mu = -1.2$ as indicated by their zero values as $1/L \rightarrow 0$.

the system size L . We then find all the eigenvalues and eigenvectors of $U(T,0)$. Since the system is invariant under parity \mathcal{P} (corresponding to reflecting the system about its mid-point), we can choose the eigenvectors of $U(T,0)$ to also be eigenvectors of \mathcal{P} .

The bulk Floquet operator U_F for periodic δ -function kicks can be written as a product of three terms: a kicked evolution with a chemical potential $V\delta(t-T)$ followed by an evolution via the free Hamiltonian H_k with a constant chemical potential μ for time T and then again a kicked evolution with a chemical potential $V\delta(t-T)$. This symmetric choice of kicking makes the particle-hole, the chiral and the time-reversal symmetries more transparent and yields the Floquet operator U_F for each momentum

mode k as²⁷

$$U_k^F = U_k(T,0) = e^{-iV\sigma^z} e^{-iH_k T} e^{-iV\sigma^z}. \quad (14)$$

The Floquet Hamiltonian H_k^F can now be obtained from U_k^F as

$$H_k^F = \frac{i}{T} \ln U_k^F \equiv E_k^F \hat{c}_k \cdot \vec{\sigma}, \quad (15)$$

where the Floquet quasienergy E_k^F defined within the Floquet Brillouin zone $-\pi/T$ to π/T and the unit vector \hat{c}_k are given by

$$E_k^F = \frac{1}{T} \arccos \left[\cos(2V) \cos(E_k T) - \frac{a_3}{E_k} \sin(2V) \sin(E_k T) \right], \quad (16)$$

$$\hat{c}_k = \frac{1}{\sin(E_k^F T)} \left\{ \frac{a_2}{E_k} \sin(E_k T) \hat{y} + \left[\sin(2V) \cos(E_k T) - \frac{a_3}{E_k} \cos(2V) \sin(E_k T) \right] \hat{z} \right\}, \quad (17)$$

where $a_2 = -f_\alpha(k)$ and $a_3 = \cos(k) - \mu$.

The same symmetrized Floquet evolution can also be carried out for the real-space Hamiltonian, but here the Floquet eigenvalues and eigenvectors have to be obtained numerically from the real-space Floquet operator $U_r^F = U_r(T,0)$. We also note that the eigenvalues of the unitary operator $U_r(T,0)$ for both open and periodic boundary conditions are given by phases, $e^{i\theta_j}$, and these must come in complex conjugate pairs if $e^{i\theta_j} \neq \pm 1$ ²⁷. This is because $U_r(T,0)$ is a real operator when written in terms of the Majorana operators a_m in Eq. (3). Hence $U_r(T,0)\psi_j = e^{i\theta_j}\psi_j$ implies that $U_r(T,0)\psi_j^* = e^{-i\theta_j}\psi_j^*$.

V. RESULTS

We can see from Eq. (16) that the bulk gap for the Floquet spectrum can close (i.e., $E_k^F T$ can be equal to 0 or π) only at $k = 0$ or π . Moreover, $E_k^F T$ in Eq. (16) can close at $E_k^F T = 0$ and π for $k = 0$ only when $\alpha > 1$ and for $k = \pi$ for any value of α . Therefore, to investigate the possible topological phase boundaries, we solve $E_k^F T = 0, \pi$ at $k = 0, \pi$, for various values of μ keeping the values of the kicking frequency $\omega = 2\pi/T$ and strength V fixed. In the rest of this section, we will refer to $E_k^F T$, rather than E_k^F , as the Floquet quasienergy; we note that $E_k^F T$ is dimensionless and lies in the range $[-\pi, \pi]$.

When $\alpha > 1$, we find that $E_k^F T = 0$ can occur if

$$\mu = \pm 1 - \frac{\omega}{\pi} [V - n\pi], \quad (18)$$

where $n = 0, \pm 1, \pm 2, \dots$, and the \pm in Eq. (18) stands for modes with $k = 0$ and π respectively. On the other hand, for $\alpha < 1$, although $E_k^F T = 0$ for $k = \pi$ for the same values of μ as above, $E_k^F T$ never crosses 0 at $k = 0$ due to the divergence of the polylogarithm function $f_\alpha(k)$ at that value of k .

Similarly, when the gap in the Floquet quasienergy $E_k^F T$ closes at $E_k^F T = \pi$, we obtain equations for the critical values of μ exactly as above. When $\alpha > 1$, we find that $E_k^F T = \pi$ for

$$\mu = \pm 1 - \frac{\omega}{\pi} \left[V - \left(n + \frac{1}{2} \right) \pi \right]; \quad n = 0, \pm 1, \pm 2, \dots, \quad (19)$$

where $n = 0, \pm 1, \pm 2, \dots$, and the \pm in Eq. (19) stands for modes with $k = 0$ and $k = \pi$ respectively. For $\alpha < 1$, although $E_k^F T = \pi$ for $k = \pi$ for the same values of μ as above, $E_k^F T$ never becomes π at $k = 0$ due to the divergence of the polylogarithm function $f_\alpha(k)$ at that value of k .

Next, we find that as we vary μ , between two successive 0 or π crossings of the quasienergy, we can have either non-topological phases with no end modes or topological phases which host massless or massive end modes at or around $E^F T = 0$ or π depending on whether $\alpha > 1$ or $\alpha < 1$ respectively. The divergence of $f_\alpha(k)$ and in turn of $E_k^F T$ at $k = 0$ for $\alpha < 1$, in fact, allows the existence of massive Dirac edge modes even for the periodically kicked system. Furthermore, we observe the following from Eqs. (18) and (19).

(i) The 0 and π crossings occur at multiple values of μ as

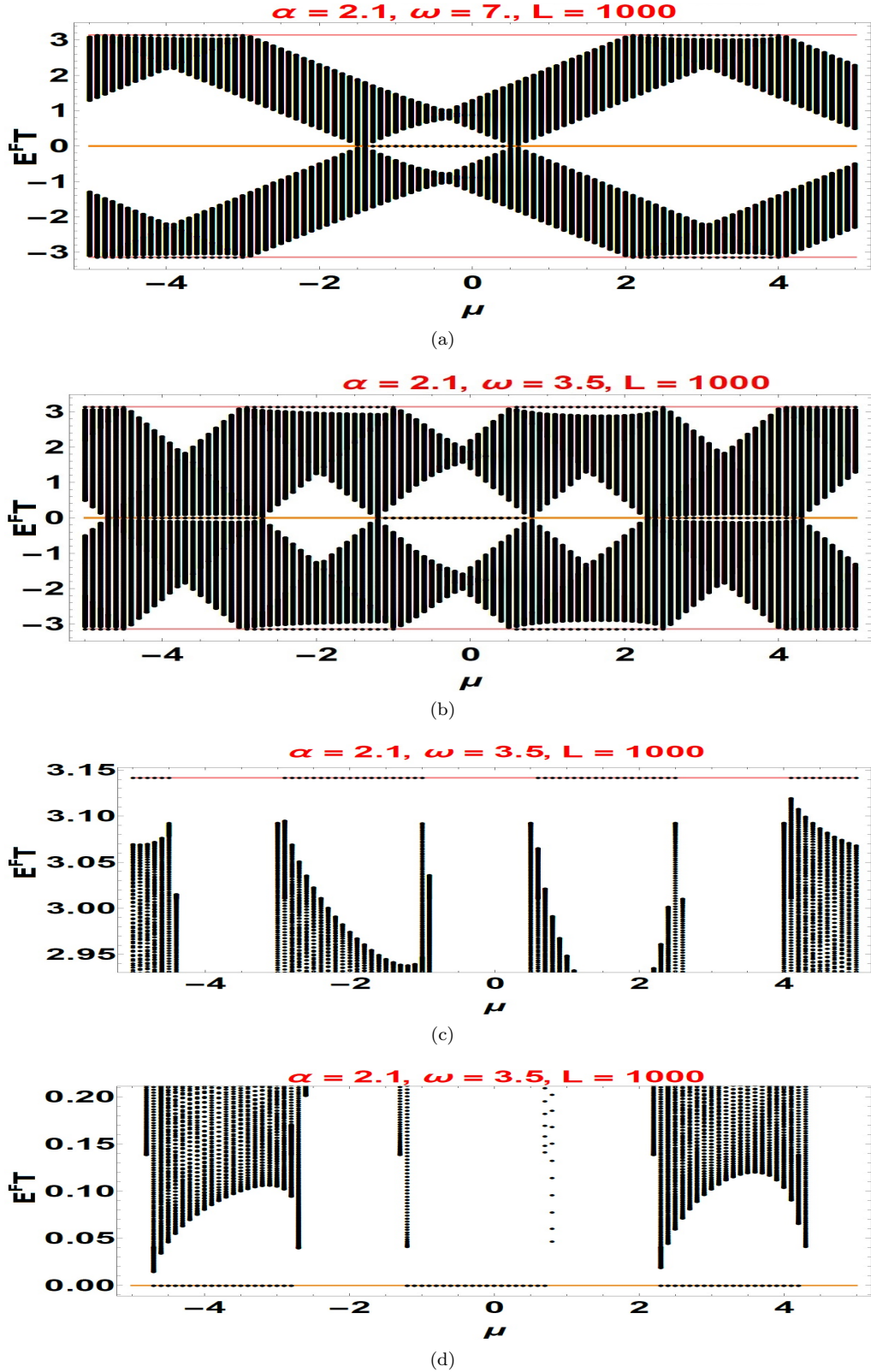


FIG. 5: Floquet quasienergy spectrum $E^F T$ of the LRK chain with open boundary conditions plotted versus the chemical potential μ for $\alpha = 2.1$, kicking strength $V = 0.2$, kicking frequencies $\omega = 7.0$ and 3.5 , and system size $L = 1000$. (a) For $\omega = 7.0$, we see that massless end modes are present at $E^F T = 0$ and π for certain ranges of values of μ where there are no end modes in the undriven energy spectrum. However, end modes at $E^F T = 0$ and π do not appear together at any value of μ . (b) For $\omega = 3.5$, massless end modes are present at $E^F T = 0$ and π for certain ranges of μ which are different from (a). We see here that massless end modes at $E^F T = 0$ and π can appear together for some values of μ , for instance, $\mu = -0.9$. For $\omega = 3.5$, the quasienergy spectrum has been zoomed around (c) $E^F T = \pi$ and (d) $E^F T = 0$. They show that the modes are truly massless, and also that massless end modes at $E^F T = 0$ and π can co-exist at certain values of μ , such as $\mu = -0.9$.

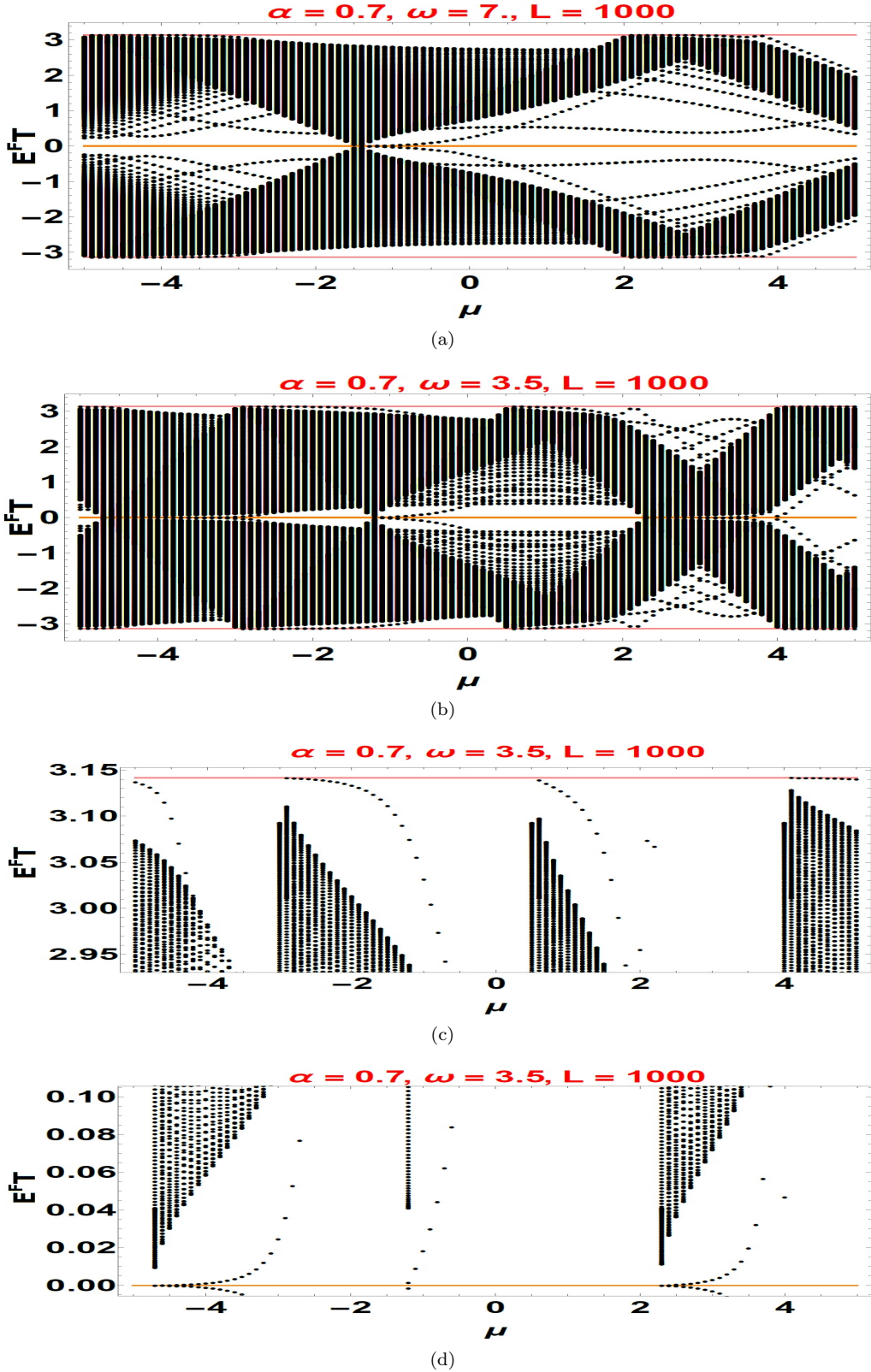


FIG. 6: Floquet quasienergy spectrum $E^F T$ of the LRK chain with open boundary conditions plotted versus μ for $\alpha = 0.7$, kicking strength $V = 0.2$, kicking frequencies $\omega = 7.0$ and 3.5 , and system size $L = 1000$. (a) For $\omega = 7.0$, we see that massive end modes are present around $E^F T = 0$ and π for certain ranges of values of μ where there are no end modes in the undriven energy spectrum. (b) For $\omega = 3.5$, massive end modes are present around $E^F T = 0$ and π for certain ranges of μ which are different from (a). The occurrence of massive end modes around $E^F T = 0$ and π can now appear together for some values of μ , for instance, $\mu = -1.1$. For $\omega = 3.5$, the quasienergy spectrum has been zoomed around (c) $E^F T = \pi$ and (d) $E^F T = 0$. They show that the modes are truly massive, and also that massless end modes at $E^F T = 0$ and π can co-exist at certain values of μ , such as $\mu = -1.1$.

the number n in Eqs. (18) and (19) hits different integer values.

(ii) The multiple crossings at $E^F T = 0$ and π result in the appearance of topological phases for certain ranges of μ which are topologically trivial in the undriven system.

(iii) The gaps $\Delta\mu$ between 0 or π crossings increase as the frequency ω increases.

(iv) On decreasing ω , the gaps $\Delta\mu$ between 0 and π crossings decrease, and we then find that are regions of μ where end modes at and around $E^F T = 0$ and $E^F T = \pi$ co-exist.

We now discuss the Floquet quasienergy spectrum $E^F T$ of the LRK chain with open boundary conditions for the two cases $\alpha > 1$ and $\alpha < 1$. The spectrum $E^F T$ is plotted versus μ for $\alpha = 2.1$, $V = 0.2$, and two values of the kicking frequency, $\omega = 7.0$ in Fig. 5(a) and $\omega = 3.5$ in Fig. 5(b). In these figures we observe that massless end modes are present at $E^F T = 0$ and π for certain ranges of values of μ . It is worth noting that the energy spectrum of the undriven system is topologically trivial (i.e., has no MZMs) for these values of μ , for both the frequencies. However, in contrast to the $\omega = 7.0$ case where massless end modes do not appear at $E^F T = 0$ and π at the same values of μ , these two kinds of modes can co-exist for certain ranges of μ (for example, $\mu = -0.9$) for the case $\omega = 3.5$. This happens due to a decrease in the gaps $\Delta\mu$ between crossings at $E^F T = 0$ and π as ω is decreased. It is interesting to zoom into the quasienergy spectrum near $E^F T = \pi$ (see Fig. 5(c)) and $E^F T = 0$ (see Fig. 5(d)), for $\omega = 3.5$. These figures show that the modes are truly massless and also that the modes at $E^F T = 0$ and π co-exist at certain values of μ such as $\mu = -0.9$.

For the case $\alpha < 1$, we find that the Floquet quasienergy spectrum does not contain any massless modes. On plotting $E^F T$ versus μ for $\alpha = 0.7$, $V = 0.2$, and frequencies $\omega = 7.0$ in Fig. 6(a) and $\omega = 3.5$ in Fig. 6(b), we observe that massive end modes are present around $E^F T = 0$ and π for certain ranges of μ where the undriven system is topologically trivial. However, in contrast to the $\omega = 7.0$ case where massive end modes do not appear at $E^F T = 0$ and π at the same values of μ , these two kinds of modes can co-exist for certain ranges of μ (for example, $\mu = -1.1$) for the case $\omega = 3.5$. The gaps $\Delta\mu$ between crossings at $E^F T = 0$ and π decrease as ω is decreased. Once again, it is interesting to look more closely at the quasienergy spectrum near $E^F T = \pi$ (see Fig. 6(c)) and $E^F T = 0$ (see Fig. 6(d)), for $\omega = 3.5$. The plots show that the modes are truly massive and not massless as in the case $\alpha > 1$. We also observe that the modes at $E^F T = 0$ and π co-exist at certain values of μ such as $\mu = -1.1$.

VI. TOPOLOGICAL INVARIANTS

The critical phase boundaries established in Sec. V for the periodically kicked LRK chain indicate that topologically trivial or non-trivial phases can lie between successive gap closings at $E^F T = 0$ or π as we vary the system parameters such as μ . To understand better whether the system lies in a topologically trivial or non-trivial phase, it would be useful to construct bulk topological invariants which can characterize the different phases. Moreover, it would also be interesting to know if a bulk-boundary correspondence (i.e., a relation between the bulk topological invariants and the number of end modes) holds for the LRK chain. To this end, we numerically determine the number and the (massless or massive) nature of the end modes when the system belongs to a topologically non-trivial phase.

We begin our analysis by calculating the bulk winding number from the Floquet Hamiltonian in Eq. (15). The winding number is defined as

$$\nu = \frac{1}{2\pi} \oint dk \frac{\partial_k c_k^y}{c_k^z}. \quad (20)$$

We note that the winding number defined above for the periodically kicked system is meaningful only for $\alpha > 1$, and is ill-defined for $\alpha < 1$ due to the divergence of the polylogarithm function which appears inside the expressions in Eq. (16). Further, calculating the winding number analytically turns out to be extremely difficult, and numerical approaches also face problems due to the divergence of the group velocity for $\alpha < 3/2$, requiring extremely large system sizes for the results to converge.

We therefore focus our attention on a second bulk invariant (see Ref. 27) which is known to correctly give the number of end modes with $E^F T = 0$ and π for the periodically kicked Kitaev chain with only nearest-neighbor pairings ($\alpha \rightarrow \infty$). The momenta $k = 0$ and π play a crucial role in the definition of this invariant since $U_k(T, 0)$ can be equal to ± 1 at only these two values of k (here 1 denotes the 2×2 identity matrix). Eq. (14) shows that only for $\alpha > 1$ when there is no divergence in the polylogarithm function, we have $U_{k=0}(T, 0) = e^{i\pi b_0 \sigma^z}$ and $U_{k=\pi}(T, 0) = e^{i\pi b_\pi \sigma^z}$ since $f_\alpha(k) = 0$ for $k = 0, \pi$. Defining $b_{0/\pi}$ in the simplest possible way, we obtain

$$\begin{aligned} b_0 &= \frac{2(\mu - 1)}{\omega} + \frac{2V}{\pi}, \\ b_\pi &= \frac{2(\mu + 1)}{\omega} + \frac{2V}{\pi}, \end{aligned} \quad (21)$$

where $\omega = 2\pi/T$. Note that b_π is always larger than b_0 . We also observe that the expressions in Eq. (21) do not depend on the value of α .

We can now see that the number of integers lying between b_0 and b_π for a fixed value of μ , V and ω serves as a bulk topological invariant for the system with $\alpha > 1$. It is clear that this number is a topological invariant since

it does not change under small deformations of the system parameters. This number can change only at values of ω where either b_0 or b_π in Eq. (21) becomes equal to an integer. When that happens, Eq. (14) becomes equal to ± 1 at either $k = 0$ or π . We therefore define a bulk topological invariant B as

$$B = [b_\pi] - [b_0], \quad (22)$$

where the floor function $[x]$ denotes the largest integer less than or equal to a real number x . The difference between the floor of b_π and the floor of b_0 therefore counts the number of integers lying within the range $[b_0, b_\pi]$.

In Figs. 7, we compare the number of massless end modes $N = N_\pi + N_0$ (where N_0 and N_π denote the numbers of massless end modes with $E^F T = 0$ and π respectively at each end an open chain and the bulk invariant B as functions of ω , for a 5000-site system with $\gamma = 1$, $\Delta = -1$, $\mu = 0.65$, $V = 0.2$, and (a) $\alpha = 2.1$ and (b) $\alpha = 1.49$. We see that the number of end modes at each end of the chain completely agrees with B in the entire ranges of ω shown in the two figures. We also note that in the limit $\omega \rightarrow \infty$ (i.e., $T \rightarrow 0$), Eq. (14) becomes independent of k ; further, Eq. (21) shows that $b_\pi \rightarrow b_0$ when $\omega \rightarrow \infty$, hence $B = 0$. This agrees with the observation that there is a maximum value of ω beyond which there are no massless end modes in both the figures.

In Figs. 7, the number of Majorana end modes for $\omega < 3$ has not been shown. As ω decreases, we see from the expression in Eq. (22) that the number of end modes increases. However, due to the presence of the long-range pairings, it becomes more and more difficult to identify the massless end modes as ω becomes small since we require larger and larger system sizes to confirm if all these end modes are really massless with Floquet eigenvalues equal to ± 1 and if these are separated from all the other eigenvalues by finite gaps.

There is a further refinement of the topological invariant in Eq. (22) which can tell us the individual values of N_0 and N_π , i.e., the number of massless modes with $E_F T = 0$ and π respectively at each end of the chain. Namely, we find that the number of even and odd integers lying within the range $[b_0, b_\pi]$ is equal to N_0 and N_π respectively; the reason for this connection is explained in Ref. 27. This is illustrated in Fig. 8 where we show plots of b_0 (bottom red line) and b_π (top blue curve) versus ω , for a 5000-site chain with $\alpha = 1.49$, $\mu = 0.65$ and $V = 0.2$. A horizontal black line showing $2V/\pi$ has been added as a reference. In agreement with Eq. (21), we see that b_0 crosses and goes below 0 at $\omega = 5.498$, while b_π crosses and goes above 1 at $\omega = 3.782$. Hence the number of even integers between b_0 and b_π is 1 from $\omega = 3$ to 5.498, and the number of odd integers between b_0 and b_π is 1 from $\omega = 3$ to 3.782. This is found to agree completely with the number of massless modes N_0 and N_π at each end of the LRK chain. We have only studied values of ω equal to integers and half-odd-integers, and we find that N_0 is equal to 1 from $\omega = 3$ to 5 and N_π is equal to 1 from $\omega = 3$ to 3.5. The total number of massless

end modes, $N_0 + N_\pi$, agrees with the results shown in Fig. 7(b).

VII. DISCUSSION

In this paper, we have considered the Kitaev chain with long-range superconducting pairing whose strength decays as a power-law with an exponent α . Depending upon the value of α , the chain hosts massless Majorana or massive Dirac modes at its ends. Using exact diagonalization of large systems, we have established that the model is topologically similar to the conventional Kitaev chain with only nearest-neighbor pairing (which arises in the limit $\alpha \rightarrow \infty$) and therefore has the same topological phase diagram in the $\mu - \alpha$ plane for all $\alpha > 1$, not just $\alpha > 3/2$. For $\alpha > 1$, the system has massless Majorana modes at the two ends of the system. For $\alpha < 1$, the system has a topological phase which is characterized by a fractional winding number and has exotic massive Dirac modes with a non-local character. These modes arise because the long-range pairing couples the would-be massless modes at the two ends of the chain; this hybridization breaks the two-fold degeneracy at zero energy and produces massive modes with non-zero energies of the form $\pm E$.

Next we investigate the non-equilibrium dynamics of this system with long-range pairings by subjecting the chemical potential μ to periodic δ -function kicks such that the time-reversal symmetry remains intact. We study the quasienergy spectrum as a function of μ for various values of the system parameters and find that both the massless Majorana (for $\alpha > 1$) and massive Dirac (for $\alpha < 1$) end modes exist but only for very large system sizes. Interestingly, the Floquet dynamics generates new massless and massive end modes at quasienergy π/T in addition to the modes near zero energy which are present in the absence of periodic kicks. Moreover, these new end modes are separated from all the other eigenvalues by finite gaps, and are therefore topologically robust. Furthermore, on varying the kicking frequency ω , we find that some topological phases can emerge in which the massless or massive end modes at quasienergies 0 and π/T can co-exist. We have found the critical values of μ which separate the non-topological and topological phases.

Motivated by the existence of bulk topological invariants (such as winding number) which can predict the number of massless Majorana end modes for a system with a time-independent Hamiltonian, we have studied if the periodically kicked system also has topological invariants which can correctly predict the number of end modes, at least for $\alpha > 1$. For $1 < \alpha < 3/2$, it turns out to be extremely difficult to compute the winding number for the periodically kicked system, both analytically and numerically (the latter method fails because the group velocity diverges if $\alpha < 3/2$, requiring extremely large system sizes for the calculations to converge). Moreover,

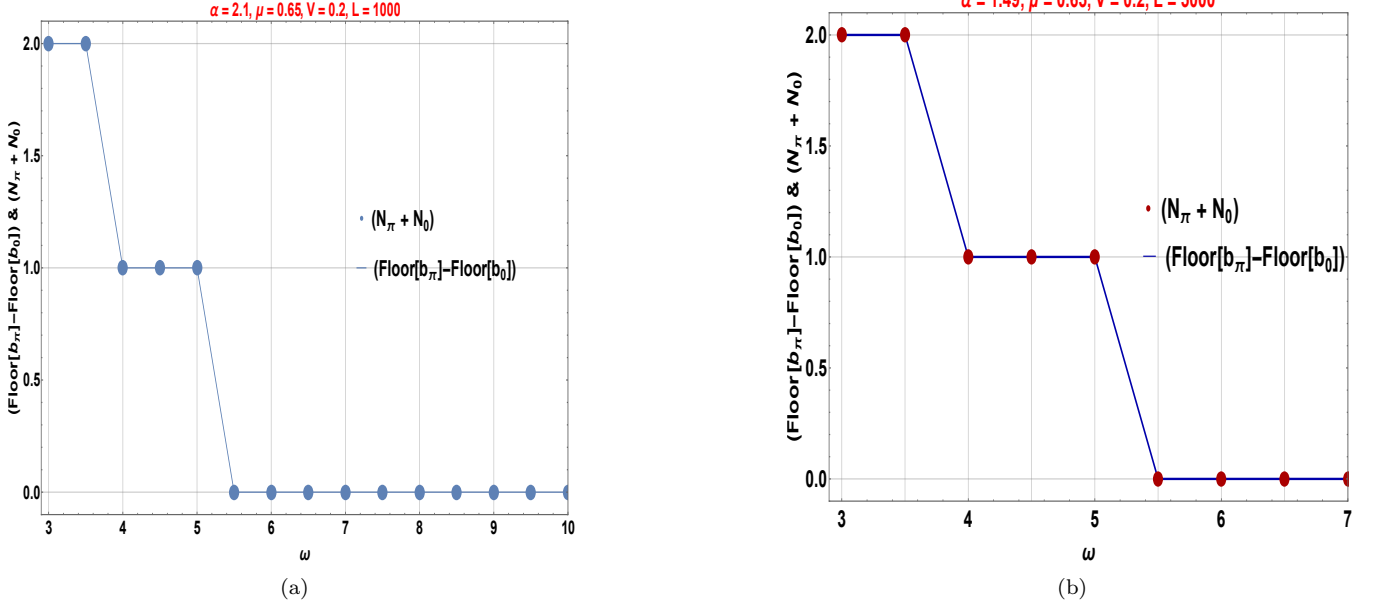


FIG. 7: (a) Comparison between the analytical plot of $\text{Floor}[b_\pi] - \text{Floor}[b_0]$ (blue solid line) and the total number of massless end modes $N = N_0 + N_\pi$ (blue dots) versus ω , for a 5000-site chain with $\mu = 0.65$, $V = 2$, and (a) $\alpha = 2.1$ and (b) $\alpha = 1.49$.

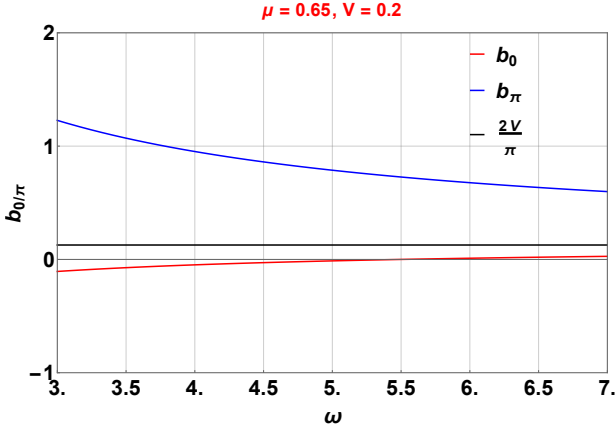


FIG. 8: Plots of b_0 (bottom red line) and b_π (top blue curve) versus ω , for a 5000-site chain with $\alpha = 1.49$, $\mu = 0.65$ and $V = 0.2$. A horizontal black line showing $2V/\pi$ has been added as a reference.

for $\alpha < 1$, the winding number calculation becomes ill-defined due to the divergence of the polylogarithm function for the zero momentum mode. We therefore use a different topological invariant, first introduced in Ref. 27, which is easy to calculate and correctly predicts the number of end modes of the kicked system, provided that $\alpha > 1$. We have shown that this topological invariant

not only gives us the total number of end modes with Floquet eigenvalues equal to $+1$ and -1 for all values of the system parameters but also provides a simple condition which can predict the values of ω at which end modes appear or disappear. In addition, we have found that this invariant can be written as a sum of two topological invariants which correctly predict the numbers of end modes with Floquet eigenvalues equal to $+1$ and -1 separately. All these topological invariants fail to work when $\alpha < 1$ where the long-range pairings become dominant. Finding a topological invariant which can predict the number of massive end modes for a periodically kicked system with $\alpha < 1$ would thus be an interesting and challenging problem for future study. For $\alpha < 1$, it would also be useful to understand how the energies (quasienergies) of the massive end modes of the undriven (periodically driven) system scale with μ close to the various phase transition points.

Acknowledgments

D.S. thanks DST, India for Project No. SR/S2/JCB-44/2010 for financial support. A.D. acknowledges SERB, DST, India for financial support.

¹ M. Z. Hasan and C. L. Kane, Rev. Mod. Phys. **82**, 3045 (2010).

² X.-L. Qi and S.-C. Zhang, Rev. Mod. Phys. **83**, 1057

- (2011).
- ³ L. Fidkowski and A. Kitaev, Phys. Rev. B **83**, 075103 (2011).
 - ⁴ T. Kitagawa, E. Berg, M. Rudner, and E. Demler, Phys. Rev. B **82**, 235114 (2010).
 - ⁵ N. H. Lindner, G. Refael, and V. Galitski, Nature Phys. **7**, 490 (2011).
 - ⁶ L. Jiang, T. Kitagawa, J. Alicea, A. R. Akhmerov, D. Pekker, G. Refael, J. I. Cirac, E. Demler, M. D. Lukin, and P. Zoller, Phys. Rev. Lett. **106**, 220402 (2011).
 - ⁷ Z. Gu, H. A. Fertig, D. P. Arovas, and A. Auerbach, Phys. Rev. Lett. **107**, 216601 (2011).
 - ⁸ T. Kitagawa, T. Oka, A. Brataas, L. Fu, and E. Demler, Phys. Rev. B **84**, 235108 (2011).
 - ⁹ N. H. Lindner, D. L. Bergman, G. Refael, and V. Galitski, Phys. Rev. B **87**, 235131 (2013).
 - ¹⁰ M. Trif and Y. Tserkovnyak, Phys. Rev. Lett. **109**, 257002 (2012).
 - ¹¹ A. Russomanno, A. Silva, and G. E. Santoro, Phys. Rev. Lett. **109**, 257201 (2012).
 - ¹² V. M. Bastidas, C. Emary, G. Schaller, and T. Brandes, Phys. Rev. A **86**, 063627 (2012).
 - ¹³ V. M. Bastidas, C. Emary, B. Regler, and T. Brandes, Phys. Rev. Lett. **108**, 043003 (2012).
 - ¹⁴ M. Tomka, A. Polkovnikov, and V. Gritsev, Phys. Rev. Lett. **108**, 080404 (2012).
 - ¹⁵ A. Gomez-Leon and G. Platero, Phys. Rev. B **86**, 115318 (2012), and Phys. Rev. Lett. **110**, 200403 (2013).
 - ¹⁶ B. Dóra, J. Cayssol, F. Simon, and R. Moessner, Phys. Rev. Lett. **108**, 056602 (2012).
 - ¹⁷ D. E. Liu, A. Levchenko, and H. U. Baranger, Phys. Rev. Lett. **111**, 047002 (2013).
 - ¹⁸ Q.-J. Tong, J.-H. An, J. Gong, H.-G. Luo, and C. H. Oh, Phys. Rev. B **87**, 201109(R) (2013).
 - ¹⁹ M. S. Rudner, N. H. Lindner, E. Berg, and M. Levin, Phys. Rev. X **3**, 031005 (2013).
 - ²⁰ J. Cayssol, B. Dóra, F. Simon, and R. Moessner, Phys. Status Solidi RRL **7**, 101 (2013).
 - ²¹ Y. T. Katan and D. Podolsky, Phys. Rev. Lett. **110**, 016802 (2013).
 - ²² A. Kundu and B. Seradjeh, Phys. Rev. Lett. **111**, 136402 (2013).
 - ²³ V. M. Bastidas, C. Emary, G. Schaller, A. Gómez-León, G. Platero, and T. Brandes, arXiv:1302.0781v2.
 - ²⁴ T. L. Schmidt, A. Nunnenkamp, and C. Bruder, New J. Phys. **15**, 025043 (2013).
 - ²⁵ A. A. Reynoso and D. Frustaglia, Phys. Rev. B **87**, 115420 (2013).
 - ²⁶ C.-C. Wu, J. Sun, F.-J. Huang, Y.-D. Li, and W.-M. Liu, EPL **104**, 27004 (2013).
 - ²⁷ M. Thakurathi, A. Patel, D. Sen, and A. Dutta, Phys. Rev. B **88**, 155133 (2013).
 - ²⁸ M. C. Rechtsman, J. M. Zeuner, Y. Plotnik, Y. Lumer, D. Podolsky, S. Nolte, F. Dreisow, M. Segev, and A. Szameit, Nature (London) **496**, 196 (2013).
 - ²⁹ A. Kitaev, Phys. Usp. **44**, 131 (2001).
 - ³⁰ S. Saha, S. N. Sivarajan, and D. Sen, Phys. Rev. B **95**, 174306 (2017).
 - ³¹ V. Mourik, K. Zuo, S. M. Frolov, S. R. Plissard, E. P. A. M. Bakkers, and L. P. Kouwenhoven, Science **336**, 1003 (2012); L. P. Rokhinson, X. Liu, and J. K. Furdyna, Nature Physics **8**, 795 (2012); M. T. Deng, C. L. Yu, G. Y. Huang, M. Larsson, P. Caroff, and H. Q. Xu, Nano Lett. **12**, 6414 (2012); A. Das, Y. Ronen, Y. Most, Y. Oreg, M. Heiblum, and H. Shtrikman, Nature Phys. **8**, 887 (2012); A. D. K. Finck, D. J. Van Harlingen, P. K. Mohseni, K. Jung, and X. Li, Phys. Rev. Lett. **110**, 126406 (2013); S. Nadj-Perge, I. K. Drozdov, J. Li, H. Chen, S. Jeon, J. Seo, A. H. MacDonald, B. A. Bernevig, and A. Yazdani, Science **346**, 602 (2014).
 - ³² D. Vodola, L. Lepori, E. Ercolessi, A. V. Gorshkov, and G. Pupillo, Phys. Rev. Lett. **113**, 156402 (2014).
 - ³³ D. Vodola, L. Lepori, E. Ercolessi, and G. Pupillo, New J. Phys. **18**, 015001 (2016).
 - ³⁴ O. Viyuela, A. Rivas, and M. A. Martin-Delgado, Phys. Rev. Lett. **112**, 130401 (2014), and Phys. Rev. Lett. **113**, 076408 (2014).
 - ³⁵ O. Viyuela, D. Vodola, G. Pupillo, and M. A. Martin-Delgado, Phys. Rev. B **94**, 125121 (2016).
 - ³⁶ Z. Huang and D. P. Arovas, Phys. Rev. Lett. **113**, 076407 (2014); O. Viyuela, A. Rivas, and M. A. Martin-Delgado, 2D Mater. **2**, 034006 (2015).
 - ³⁷ H.-J. Stöckmann, *Quantum Chaos* (Cambridge University Press, Cambridge, 1999).
 - ³⁸ A. P. Schnyder, S. Ryu, A. Furusaki, and A. W. W. Ludwig, Phys. Rev. B **78**, 195125 (2008).
 - ³⁹ A. Kitaev, in *Advances in Theoretical Physics: Landau Memorial Conference*, edited by V. Lebedev and M. Feigel'man, (AIP, 2009).
 - ⁴⁰ M. V. Berry, Proceedings of the Royal Society of London, Series A, **392**, 45 (1984).
 - ⁴¹ Y. Aharonov and J. Anandan, Phys. Rev. Lett. **58**, 1593 (1987).
 - ⁴² J. Zak, Phys. Rev. Lett. **62**, 2747 (1989).